scientific reports

Check for updates

OPEN

Edaravone dexborneol provides neuroprotective benefits by suppressing ferroptosis in experimental intracerebral hemorrhage

Han Li[1,2,7], Xiang Li[3,6,7], Mingzhi Li[1,2], Wenxin Li[3], Jinghui Wei[4,5], Yuming Huang[1,2], Haiqing Yan[3], Juntang Lin[2]✉ & Ping Zhang[3]✉

Edaravone dexborneol (EDB) is widely recognized for its anti-inflammatory and antioxidant properties and is clinically applied in the treatment of acute cerebral infarction. Ferroptosis is a critical process in the pathophysiology of brain injury following intracerebral hemorrhage (ICH). However, it remains unclear whether EDB can ameliorate ICH through the modulation of ferroptosis. This study aimed to evaluate the function and mechanism of EDB in treatment of ICH. With a male rat ICH model, animal behavior tests, histopathological staining, magnetic resonance imaging and evans blue staining were used to evaluate the neural protective function of EDB on ICH rats. The potential molecular mechanism was investigated using RNA sequencing. With the administration of Fer-1, a range of ferroptosis-related biomarkers, including Fe^{2+}, 4-hydroxynonenal, malondialdehyde, etc., were analyzed to ascertain whether EDB confers neuroprotective effects through the modulation of P53/GPX4 pathways to inhibit ferroptosis. Finally, the findings were further corroborated using an in vitro ICH model with a P53 inhibitor. EDB has the potential to markedly enhance nerve and motor function, mitigate pathological damage, facilitate hematoma clearance, and repair BBB injury in ICH rats. KEGG analysis revealed that the differentially expressed genes were associated with signaling pathways, including P53 and ferroptosis. Both EDB and Fer-1 substantially reduced the concentrations of Fe^{2+}, 4-hydroxynonenal, malondialdehyde, increased the amount of anti-oxidants, decreased the expression of P53, and concurrently upregulated the expression of GPX4. Besides, the P53 inhibitor PFT-α was observed to significantly reduce the levels of 4-HNE and lipid peroxides, while concurrently increasing the expression of GPX4. This investigation has shed light on the crucial neuroprotective role of EDB by regulating ferroptosis in ICH disease, which provided a theoretical basis for the clinical application of EDB in the treatment of ICH.

Keywords Edaravone dexborneol, Intracerebral hemorrhage, Ferroptosis, P53, GPX4

Intracerebral hemorrhage (ICH) is caused by bleeding blood vessels and represents about 15% of all stroke cases[1]. ICH-induced brain injury is conventionally divided into two subtypes: primary brain injury and secondary brain injury. The influx of blood ooze into the brain parenchyma form hematoma and lead to surrounding tissue oppression, which is the primary injury of ICH. The secondary brain injury consists of a series of pathological process such as toxicity of hematoma metabolites, oxidative stress, inflammation, and neuronal apoptosis[2–4]. A growing number of studies have shown that multiple cell death pathways, such as apoptosis, necrosis, and pyroptosis are involved in the pathological process and development of cerebral hemorrhage[5,6]. The precise

[1]School of Life Science and Technology, Xinxiang Medical University, Xinxiang 453003, China. [2]Stem Cell and Biotherapy Engineering Research Center of Henan, Xinxiang Medical University, Xinxiang 453003, China. [3]Department of Neurology, The First Affiliated Hospital of Xinxiang Medical University, Xinxiang 45003, China. [4]School of Life Sciences, Zhengzhou University, Zhengzhou 450001, China. [5]Tianjian Laboratory of Advanced Biomedical Sciences, Zhengzhou University, Zhengzhou 450001, China. [6]Henan Department of Neurology, Henan Key Laboratory of Neural Regeneration and Repairment, Xinxiang, China. [7]Han Li and Xiang Li contributed equally to this work. ✉email: linjtlin@126.com; zhangpingsjnk@163.com

mechanisms of cell death in the perihematoma tissues remain unclear. Current clinical interventions primarily focus on surgical evacuation of hematomas, alleviation of mechanical compression, and management of primary brain tissue damage[7]. However, limited advancements have been achieved in addressing secondary brain injuries resulting from various hematoma constituents. Notably, secondary brain injury encompasses white matter damage, inflammatory responses, and neuronal loss, which significantly impacts patient prognosis following ICH[8].

Ferroptosis is an iron-dependent form of cell death characterized by iron homeostasis disruption, glutathione peroxidase 4 (GPX4) inactivation, and lipid peroxide augmentation[1,4]. At the onset of ICH, multiple blood components, including erythrocytes, leukocytes, and platelets, leach into the brain. Erythrocytes are phagocytized by macrophages, releasing hemoglobin (Hb). Heme oxygenase-1 (HO-1) catalyzes the oxidative degradation of Hb to free iron, carbon monoxide (CO), and biliverdin[8,9]. The deposited iron and hydrogen peroxide cause the Fenton reaction in the cell to produce a large concentration of highly toxic hydroxyl radicals. These hydroxyl radicals cause the peroxidation of unsaturated fatty acids on the surface of cell membranes, subsequently leading to programmed cell death[10]. Liu et al.. conducted differential gene analysis on the sequencing results of perihematoma tissues of ICH patients and contralateral corresponding parts, and then intersected with the ferroptosis database. Their findings revealed a set of 45 differentially expressed genes that are closely associated with the pathogenesis and progression of ferroptosis[11,12]. Iron chelation or ferroptosis inhibitors have shown efficacy in preclinical ICH studies[5,10]. Targeting ferroptosis inhibition as a therapeutic approach may represent a promising strategy for mitigating secondary brain injury following ICH.

Edaravone dexborneol (EDB) is a clinically effective neuroprotective agent configured from edaravone and borneol in the ratio of 4:1. It has been reported to play a protective role in diseases such as colitis, amyotrophic lateral sclerosis, experimental subarachnoid hemorrhage and ischemic stroke by inhibiting inflammation, apoptosis, pyroptosis, and anti-oxidation[13–16]. However, to our knowledge, there is no report that describes the therapeutic effects of EDB on ferroptosis at an early period after intracerebral hemorrhage insult. Therefore, in this experiment, we aimed to investigate whether EDB treatment could improve early ICH outcomes and to elucidate which responding signaling pathways are associated with the protective effect of EDB. We hypothesize that EDB could provide neuroprotective benefits by suppressing P53/GPX4-mediated ferroptosis in experimental ICH model.

Methods

Animals and ethics

Adult wild type male Sprague-Dawley (SD) rats, weighing 250–300 g, aged 8–9 weeks, were purchased from Beijing Vital River Laboratory Animal Technology Co., Ltd. (Beijing, China; License No. SCXK (Jing) 2016-0011). Rats were housed under standard laboratory conditions with 12 h light/dark cycle, 23 ± 2 ℃, and 45–60% humidity. Rats were watered and fed ad libitum. A total of 190 rats were used in the experiment. For animal related experiments, each group included 5 rats, except for behavior test, which included 10 rats in Sham group, 15 rats in ICH or EDB group. All experimental data were collected and analyzed in a blinded fashion; the operator and designer were blinded to each other.

All protocols for the animal experiments were registered and approved by the Ethics Committee of Xinxiang Medical University (XYLL-20240254). All methods were performed in accordance with ARRIVE guidelines and regulations (https://arriveguidelines.org). All methods were performed in accordance with the relevant guidelines and regulations.

ICH model construction

Rats were randomly divided into Sham group ($n = 48$) and ICH group ($n = 116$) by lottery method. After anesthetized by intraperitoneal injection of pentobarbital sodium (45 mg/kg), ICH model was induced by stereotaxic infusion of *Clostridium histolyticum* collagenase VII (0.2 U in 1.0 μL sterile saline, Sigma-Aldrich) into right striatum as a speed of 0.1 μL/min. According to the brain atlas written by Paxinos and Watson[17], the stereoscopic coordinates were 3.0 mm lateral and 0.5 mm anterior to the bregma, at a depth of 5.5 mm from the bone surface. To prevent backflow, the needle was held in situ for 10 min after injection and then slowly removed. The Sham group rats were treated via the same way except that they were administrated 1 μL sterile saline into the right striatum. All rats were assessed by Zea Longa as described below. The failed Sham or ICH group rats were eliminated immediately and spare rats were used for model construction. All rats were allowed to recover in separate cages with free access to food and water.

Zea longa behavior test

Once rats were totally recovered from the anesthesia of ICH surgery (around 6 h after ICH onset), the Zea Longa behavior test was performed to evaluate whether the Sham or ICH rat model was successful or not. The 5 scoring criteria of Zea Longa was described as follows: 0 means the absence of nerve deficit symptoms; 1 score means the front paw of the hemiplegic side cannot be fully extended; 2 score represents the turn to the hemiplegic side when walking; 3 score represents the dumping to the hemiplegic side when walking; 4 score represents the inability to walk spontaneously and loss of consciousness. For ICH group rats, a score of 1–3 was considered as successful ICH rats; Rats of 0 and 4 score were excluded from ICH group. For Sham group rats, only 0 score was considered as successful Sham rats. Successful ICH rats or Sham rats were performed following experiments. Failed ones were excluded directly.

EDB and Fer-1 treatment

The SD rats were randomly divided into 5 groups: Sham group, ICH group, EDB group, Fer-1 group, and Fer-1 + EDB group, 5 rats for each group. All groups except for the Sham group were underwent ICH surgery. For

EDB group, ICH rats were intravenously injected with EDB (Nanjing Simcere, Nanjing, China) at 1 h, 24 h, 48 h, and 72 h after surgery with a dose of 3.75 mg/kg. Fer-1 powder (cat# HY-100579, MedChem Express, New Jersey, America) were dissolved in 2% DMSO (prepared by sterile saline). For Fer-1 group, rats were administered intraperitoneally with 2 mg/kg Fer-1 immediately after ICH surgery. For Fer-1 + EDB group, after treated by Fer-1 with the same way and dose as Fer-1 group, rats were then injected with EDB at 1 h, 24 h, 48 h, and 72 h after ICH surgery with a dose of 3.75 mg/kg. Except for Fer-1 and Fer-1 + EDB groups, the other three groups should be intraperitoneally injected with the same volume of 2% DMSO immediately after ICH surgery.

Assessment of neurobehavioral function by mNSS and corner turn

Modifed neurological severity score (mNSS) and corner turn were used to evaluate the neurobehavioral function of rats by two trained investigators who were blinded to animal grouping. mNSS was performed among Sham, ICH and EDB group at 6 h, 1 day, 2days, 3 days, and 7 days after EDB or saline treatment. The mNSS is consisted of motor, sensory, balance, and reflex tests. mNSS score is graded via the scale of 1–18 points (1–6, mild injury; 7–12, moderate injury; 13–18, severe injury). For the corner-turn test, the rat was placed in a corner with a 30° angle, and the turning direction for exiting the corner was recorded. This process was performed 10 times for each rat. The proportion of rats turning to the affected side was calculated to evaluate the recovery of nerve function.

Motor behavior detection

The motor coordination ability of rats in Sham group, ICH group and EDB group were detected by rotarod test. The protocol of rotarod test was described in previously published paper[18]. Briefly, rats were placed on a six-lane rotarod treadmills (RWD, Shenzhen, China). An accelerating mode was used in this test, from 0 rpm to 20 rpm over 300 s. The duration time of rats staying on the rotarod was recorded. Each animal underwent this test 3 times with an interval of at least 20 min. The mean value from the 3 trials was recorded.

Tissue collection and processing

Three days after EDB treatment, the rats in Sham group, ICH group and EDB group were deeply anesthetized with ketamine (75 mg/kg) combined with medetomidine (0.5 mg/kg) by intraperitoneal injection. Rats were transcardially perfused with PBS and then with 4% PFA. The whole brain was then collected from each animal and transferred into a 4% PFA solution. Brain tissues were finally embedded in paraffin and sliced to 5 μm thick sections for Hematoxylin-Eosin (HE), Luxol Fast Blue (LFB), Nissl, and Prussian blue staining.

Nissl, LFB, HE and Prussian blue staining

Nissl staining was used to observe the nissl bodies in the perihematomal region. Briefly, rehydrated slices were stained with 1% toluidine blue for 10 min. The sections were rinsed with distilled water to remove the excess staining solution and then dehydrated with an ethanol gradient and mounted with neutral resin.

LFB staining was utilized to observe the myelin sheath structure in the hematoma region using a LFB staining kit (G1030, Servicebio, Wuhan, China). Slices were incubated in 0.1% Luxol Fast Blue solution for 4 h at 65 °C. After rinse in water, slices underwent differentiation by dipping in lithium carbonate solution for 2 s followed by further differentiation in alcohol reagent for 15 s. The differentiation process was halted with water rinse. Eosin was used as a counterstain. After dehydrate in absolute alcohol for 3 times, slices were cleared with xylene, and mounted with neutral resin.

HE staining was used to observe the pathological changes in the perihematomal region. Briefly, rehydrated slices were stained with hematoxylin for 5 min, and stained with eosin for 1 min. The sections were then dehydrated with an ethanol gradient, cleared with xylene, and mounted with neutral resin.

Prussian blue staining was used to detect iron accumulation within the perihematomal region. Briefly, rehydrated slices were stained with prussian blue for 15 min. The sections were rinsed with distilled water to remove the excess stain solution and then further stained with nuclear fast red for 30 s. After that, they were subjected to gradient ethanol dehydration, dimethyl benzene transparent, and then mounted with neutral resin.

After staining, all samples were observed and captured by an optical microscopy (model DMi8, Leica, Germany).

Magnetic resonance imaging (MRI) detection

MRI was used to evaluate the volume of hematoma area and bilateral ventricles on day 1 and day 3 post ICH by a 3.0 T MRI scanner (Ingenia Elition X, Philip, Netherlands) at the first affiliated hospital of Xinxiang Medical University. The T2-weighted imaging (T2WI) data was acquired using Turbo Spin Echo (TSE) sequence with the following parameters: repetition time (TR) /echo time (TE) = 2500/120 ms, field of view (FOV) = 60 × 60 mm, slice thickness = 1.0 mm, matrix size = 200 × 192. MRI post-processing was performed on an off-line workstation by two experienced neurologists who were blinded to the group set. The hematoma area and bilateral ventricles were measured using Image Pro-Plus 6.0 (National Institutes of Health, Bethesda, Maryland, USA). Hematoma volume and bilateral ventricles volume were calculated as previously described[19].

Hematoma assessment

Three days after EDB treatment, rats were deeply anesthetized with ketamine (75 mg/kg) combined with medetomidine (0.5 mg/kg) by intraperitoneal injection. Then, rats were transcardially perfused with 0.9% saline followed by 4% paraformaldehyde. Whole brain tissue was excised and cut into 0.5 mm-thick coronal sections using a vibratome (Leica, VT1200S). Based on the anatomical landmarks according to Paxino and Watson[17], for each rat, 9 slices containing striatum region were collected for imaging with a camera. The size of the hematoma was measured by Image Pro-Plus 6.0. The total hematoma volume (mm^3) was calculated by summing the clot

area in each section and multiplying by the section thickness. In other words, the total hematoma volume = 0.5* (S1+…+S9) and S represents the bleeding area.

Evaluation of blood-brain barrier integrity

The integrity of blood-brain barrier (BBB) was investigated by measuring the extravasation of Evans blue (EB) dye (cat# E2129, Sigma), according to the protocol of Hou et al.[20]. Briefly, the rats ($n = 5$ for each group) were intravenously administrated EB solution (2% in saline, 4 mL/kg) by the tain vein 72 h after the onset of ICH or EDB treatment. After a circulation of 3 h, rats were deeply anesthetized with ketamine (75 mg/kg) combined with medetomidine (0.5 mg/kg) by intraperitoneal injection and were transcardially perfused with 0.01 M cold phosphate buffer solution (PBS, pH 7.4) of 250 mL to clear EB dyes in cerebral circulation.

To detect the distribution of EB in brain, after cold PBS perfusion, rat brain tissue was collected. Brain tissue was placed in a rat brain mold (BS-375 C, CINONTECH, Beijing, China) and sliced into uniform coronal sections of about 1 mm thickness. Based on the anatomical landmarks according to Paxino and Watson[17], for each rat, 5 slices containing striatum region were collected for imaging with a camera.

To detect the amount of EB in brain, each brain sample was quickly removed after PBS perfusion and separated into left hemisphere and right hemisphere. The right hemisphere was weighed and homogenized with formamide solution using an ultrasonic homogenizer (JY92-IIN, SCIENTZ, Ningbo, China). The homogenate was incubated at 60℃ for 24 h. Subsequently, following centrifugation (15,000 rpm for 20 min), supernatant was collected and its absorbance at 620 nm was determined with an automatic microplate reader (Spectramax M5, Molecular Devices, LLC., USA). The EB leakage was represented as μg/g (brain weight).

The preparation of striatum brain tissue supernatant

At 3 d after ICH onset, the rats in Sham group, ICH group and EDB group were deeply anesthetized with ketamine (75 mg/kg) combined with medetomidine (0.5 mg/kg) by intraperitoneal injection. The striatum of brain tissue was obtained and homogenized with PBS (9 mL PBS per 1 g tissue) using tissue lyser (KZ-5 F-3D, Servicebio, Wuhan, China). Following centrifugation at 10,000 rpm for 10 min at 4 ℃, supernatant was collected. The supernatant of different samples were kept in − 80 ℃ for detection of 4-HNE, SOD, MDA, and GSH using different kits.

Cell culture and treatment

Rat pheochromocytoma (PC12) cells were purchased from Pricella (Wuhan, China) and were cultured in DMEM supplemented with 10% FBS and 1% penicillin/streptomycin, and incubated at 37 ℃ in an atmosphere of 5% CO_2. Cells between passages 4–9 were used for all experiments. PC12 cells were incubated in DMEM with 10 μM EDB or/and 25 μM PFTα for 1 h, then they were exposed to 300 μM hemin (MCE, Shanghai, China) for 3 h. The cultured PC12 cells were divided into five groups: Control group, Hemin group, EDB + Hemin group, PFTα + Hemin group and EDB + PFTα + Hemin group, and the samples of each group were retained for the following experiment.

Cell viability assay

Cell viability of cells in different groups was detected using a CCK-8 kit. 10 μl of CCK-8 solution was added to each well and the plate was incubated for 2 h at 37 °C. The absorbance at 450 nm was measured by a microplate reader.

Determination of lipid peroxidation by flow cytometry

Cells in different groups were counted and washed with PBS, then incubated with 5 μM C11-BODIPY 581/591 probe at 37 ℃ in the dark for 30 min. After washing and re-suspended with 500 μL staining buffer, a flow cytometer was used to detect the fluorescence intensity (Guava® easyCyte™, Luminex, USA).

The detection of 4-HNE by ELISA

One ELISA kit (cat# MM-925888O2, MEIMIAN, Jiangsu, China) was used to detect the amount of 4-HNE in the supernatant of striatum and cells according to the manufacturer's instruction. A microplate reader (Infinite F50, TECAN) was used for photometric measurement at 450 nm.

The measurement of T-SOD, MDA, and GSH content

Total superoxide dismutase (T-SOD) activity assay Kit (E-BC-K020-M, Elabscience), glutathione (GSH) assay kit (E-BC-K030-M, Elabscience), and malondialdehyde (MDA) assay kit (E-BC-K025-M, Elabscience) were employed for detection the levels of T-SOD, GSH and MDA in the brain tissues according to the manufacturer's instruction. Another GSH assay kit (A006-2-1, Jiancheng Bioengineering) and MDA assay kit (E-BC-K028-M, Elabscience) were employed for detection the levels of GSH and MDA of cells. A microplate reader (Epoch2, BioTek, Vermont, America) was used for photometric measurement at 450 nm, 405 nm, and 532 nm, respectively. By fitting a standard curve, T-SOD, MDA, and GSH levels were calculated.

Fe^{2+} concentration determination

Fe^{2+} colorimetric assay kits (E-BC-K773-M, E-BC-K881-M, Elabscience) were used to examine the concentration of Fe^{2+} in striatum and PC-12 cells following the manufacturer's instruction. Briefly, the striatum of brain tissue was obtained and homogenized with extracting solution using tissue lyser (KZ-5 F-3D, Servicebio, Wuhan, China). Supernatant was collected by centrifuge at 12,000×g for 10 min at 4 ℃. Then, the supernatant was incubated with iron chromogenic agent at 37 ℃ for 10 min and the sample was obtained via a 10 min

centrifugation (12,000×g). The absorbance at 593 nm wavelength was determined using a microplate reader (Epoch 2, BioTek).

Western blot assay

At 3, 7 days after ICH onset, rats were euthanized by intraperitoneal injection of 250 mg/kg pentobarbital sodium and brain was quickly detached on ice. Striatum tissue was lysed with RIPA buffer using tissue lyser (KZ-5 F-3D, Servicebio, Wuhan, China). For in vitro experiments, PC-12 cells were collected and lysed in RIPA lysis buffer directly. The protein concentration was determined using an enhanced BCA protein assay kit (P0010S, Beyotime). 15 μg of total protein were separated by SDS–polyacrylamide gel electrophoresis (SDS–PAGE) and transferred to PVDF membranes, blocked by Fast Transfer buffer (P30500, NCM Biotech) for 10 min, followed by incubation with rabbit anti-HIF-1α (1:2000, 20960-1-AP, Proteintech), rabbit anti-SLC7A11 (1:1000, DF12509, Affinity Biosciences), rabbit anti-GPX4 (1:1000, DF6701, AffinityBiosciences), rabbit anti-MMP-9 (1:2000, 10375-2-AP, Proteintech), rabbit anti-occludin (1:2000, 27260-1-AP, Proteintech), rabbit anti-ZO-1 (1:10000, 21773-1-AP, Proteintech), mouse anti-HMOX-1 (1:1000, BF8020, Affinity Biosciences), mouse anti-NRF2 (1:2000, BF8017, AffinityBiosciences), mouse anti-P53 (1:2000, 60283-2-Ig, Proteintech), mouse anti-GAPDH (66129-1-Ig, 1:5000, Proteintech) as the internal control. Primary antibodies were incubated overnight at 4 ℃ followed by HRP-conjugated secondary antibodies (A16096, Invitrogen, goat anti-rabbit, 1:10,000 or 62-6520, Invitrogen, goat anti-mouse, 1:5000) for 2 h at room temperature. Immunoblotted protein signals were visualized with ECL enhanced chemiluminescent substrate kit (WBKLS0050, Millipore) following manufacturer's instructions. Densitometry of the western blot protein bands was analyzed using Image Pro-Plus 6.0.

RNA-seq and analysis

Striatal tissue samples from rats in the Sham, ICH, and EDB groups were collected for mRNA high-throughput sequencing. RNA extraction and quality check were implemented by the sequencing service provider (Shanghai Personal Biotechnology Co.,Ltd) following standardized protocols. Specifically, RNA was isolated using TRIzol reagent (Invitrogen Life Technologies, Carlsbad, CA, USA); RNA purity and concentration was detected by Nanodrop 2000 (Thermo Scientific, Waltham, Massachusetts, USA); RNA integrity was analyzed via Agilent 2100 Bioanalyzer (Agilent Technologies Inc, California, USA). Three biological replicates were obtained for each group. Raw read counts were normalized to log2-counts per million using the calc-NormFactors function from the R package edgeR (v.3.40.2) and voom from the R package limma (v3.54.2). Differential expression genes (DEGs) between the groups were analyzed using the "Limma" package in R software version 4.2.2. Genes with a P value < 0.05 and | log2 FoldChange | > 0.58 were considered as DEGs. The figures of volcano plot, heatmap, Gene ontology (GO) and Kyoto Encyclopedia of Genes and Genomes (KEGG) enrichment analysis were generated using the "ggplots", "pheatmap", and "clusterProfiler" packages in R software.

Statistical analysis

Statistical analysis was performed using Prism 8.0.2 software (Graph-Pad, San Diego, CA, USA). Data are expressed as mean ± standard deviation (SD). Data normality was detected by Shapiro–Wilk test. Homogeneity of variance was detected by Brown–Forsythe test. For data that fit a normal distribution and homogeneity of variance, one-way ANOVA followed by Turkey test was used for statistical analysis for comparisons between multiple groups. For data that does not conform to a normal distribution, nonparametric Kruskal-Wallis test was used for comparison between multiple groups. $P < 0.05$ was considered statistically significant. Sample size was calculated using online software (Experimental design assistant; https://eda.nc3rs.org.uk/eda/login/auth). With the mNSS result as primary outcomes, if the effect size is 3 between ICH and EDB group, and variability is 1, we will need to study 5 subjects in each group to reject the null hypothesis that the population means of each group are equal with probability (power) 0.9. The Type I error probability associated with this test of this null hypothesis is 0.05. Therefore, our samples for animal work are minimum 5 for each group.

Results

Edaravone dexborneol improved the neurological function of ICH rats

In order to explore the impact of EDB on the neurological function of the ICH rats, behavioral assessments including mNSS score, rotarod test, and corner tests were performed within 7 days after ICH. The flow chart of animal experiments was shown in Fig. 1A,B. As demonstrated in Fig. 1C, in the Sham group, the mNSS scores were 0 at all time points. The mNSS scores in the remaining two groups peaked at 6 h after ICH and then gradually decreased over time. Our data showed that there was no difference in mNSS between the ICH and EDB group on the 6 h and 1 day after ICH. However, rats in ICH group exhibited a significantly more severe neurological function defect on the 2, 3, and 7 days after ICH, compared to those in EDB group ($^{###}P < 0.001$ vs. ICH group). The motor coordination ability of the rat was detected by rotarod test. As shown in Fig. 1D, the total times of fall in the rotarod test in the Sham group were higher than in the ICH and EDB group. At 2, 3, and 7 days after cerebral hemorrhage, the residence time on the rotameter was significantly lower than that in rats in the EDB group. EDB treatment significantly prolonged the latency period ($^{##}P < 0.01$ vs. ICH group; $^{###}P < 0.001$ vs. ICH group). The results depicted in Fig. 1E indicate rats with ICH showed a markedly increased frequency of right turns compared with the Sham group, presenting typical post-ICH behavioral deficits. There was no difference infrequency of right turns between the ICH and EDB group on the 1 and 3 days after ICH. However, rats in ICH group showed fewer right turns on the 7 days after ICH, compared to those in EDB group ($^{###}P < 0.001$ vs. ICH group). The results suggested EDB improved the neurological function of ICH rats.

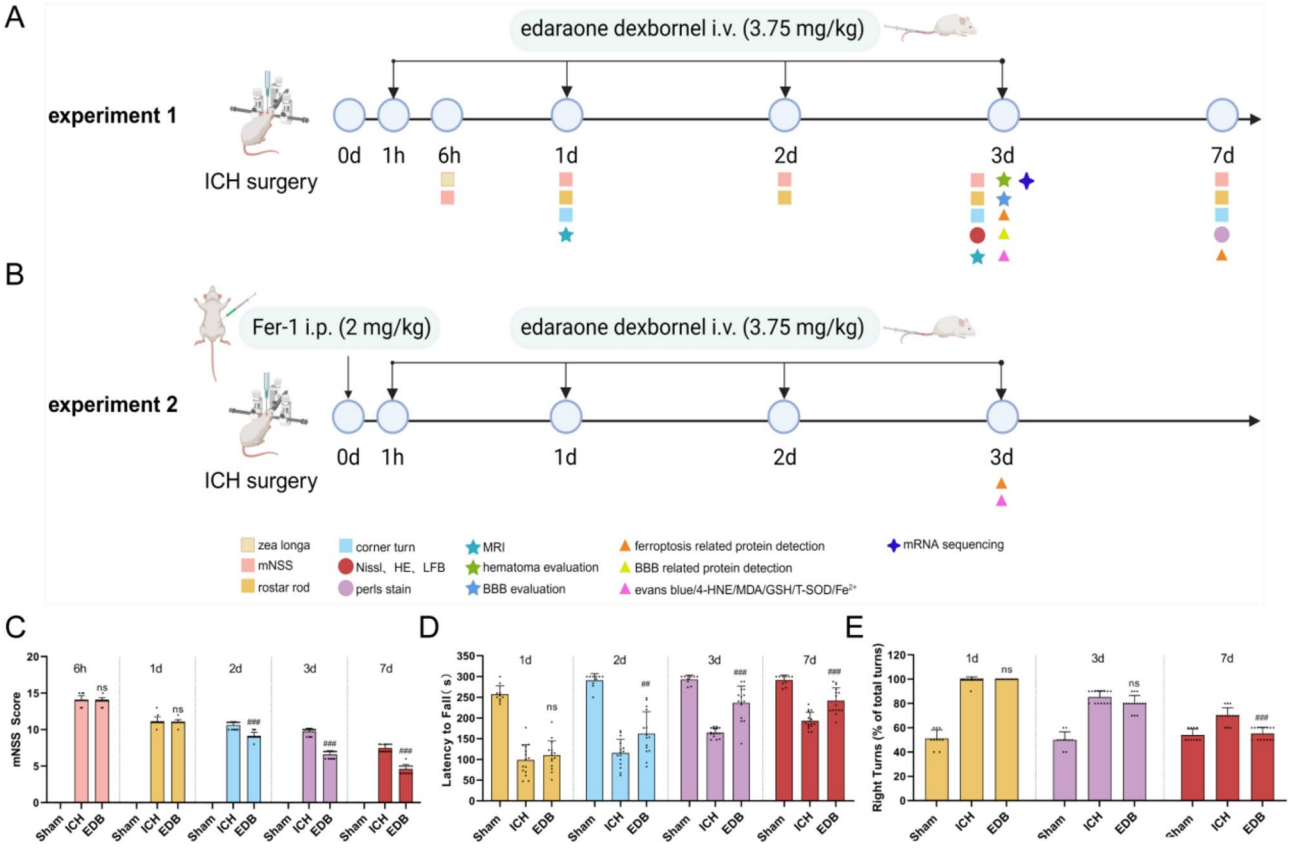

Fig. 1. Experimental design and animal behavior test. (**A**,**B**) Schematic diagram of the in vivo experimental procedure. (**C**) mNSS results assessed neurological impairment of rats. (**D**) Rotarod test results showed the duration time of rats staying on the rod. (**E**) The corner turn test show frequency of right turns in rats. $^{\#\#}P<0.01$ vs. ICH group; $^{\#\#\#}P<0.001$ vs. ICH group. $N=10$ in Sham group; $N=15$ in ICH and EDB group.

EDB reduces pathological injury and inflammation infiltration after ICH

To elucidate the pathological basis of the therapeutic effect of EDB in ICH rats, Nissl, LFB and HE staining was performed. Figure 2A–C is representative whole brain slices of different groups As shown in Fig. 2D–F, Nissl staining in the perihematomal region revealed that the cytoplasm of neuronal cells in the Sham group exhibited dark blue granular Nissl bodies, indicative of normal morphology, uniform staining, and the absence of pathomorphological alterations. Conversely, in the ICH group, neurons displayed vacuolated nuclei, karyopyknosis, reduced or absent Nissl bodies. With the treatment of EDB, most of the neurons had a fair morphology, with relatively clear nucleoli and mildly lysed Nissl bodies. LFB staining was employed to assess the structural and pathological alterations of myelin within the hematoma region. Figure 2G–I showed myelin within the Sham group exhibited a block-like distribution with distinct boundaries. Conversely, the ICH group displayed diffuse myelin loss and disintegration, characterized by a punctate and scattered distribution of myelin phospholipids. Following EDB treatment, a reduction in the extent of myelin damage was observed compared to the ICH group. The morphology and cell number in the perihematomal region were examined using HE staining, as depicted in Fig. 2J–L. The brain tissue cells in the Sham group exhibited a uniform arrangement, while the ICH group displayed numerous inflammatory cell clusters with irregular distribution. Following EDB treatment, there was a notable decrease in inflammatory cell infiltration.

Edaravone dexborneol reduced hematoma volume and lateral ventricle volume of ICH rats

On T2-weighted imaging, high signal intensity was observed in the central region of the cerebral hematoma and the lateral ventricle of rats receiving collagenase VII injection (Fig. 3A–E). The hematoma volume was quantified as depicted in Fig. 3F. On day 1, the hematoma volume in the EDB group showed a reduction compared to the ICH group, although this difference did not reach statistical significance. However, it is noteworthy that by day 3, the hematoma volume in the EDB group exhibited a reduction, whereas the ICH group displayed a continued increase. Furthermore, the hematoma volume in the EDB group was significantly lower than that in the ICH group.

Subsequently, the volume of lateral ventricles was quantified in each group to evaluate the severity of hydrocephalus. The results in Fig. 3G indicate a significant enlargement of ventricles in both the ICH and EDB groups on the initial day post-ICH, with no notable distinction between the two. By day 3, both the ICH and EDB groups exhibited smaller lateral ventricle volume than that on day 1, indicating a trend towards self-

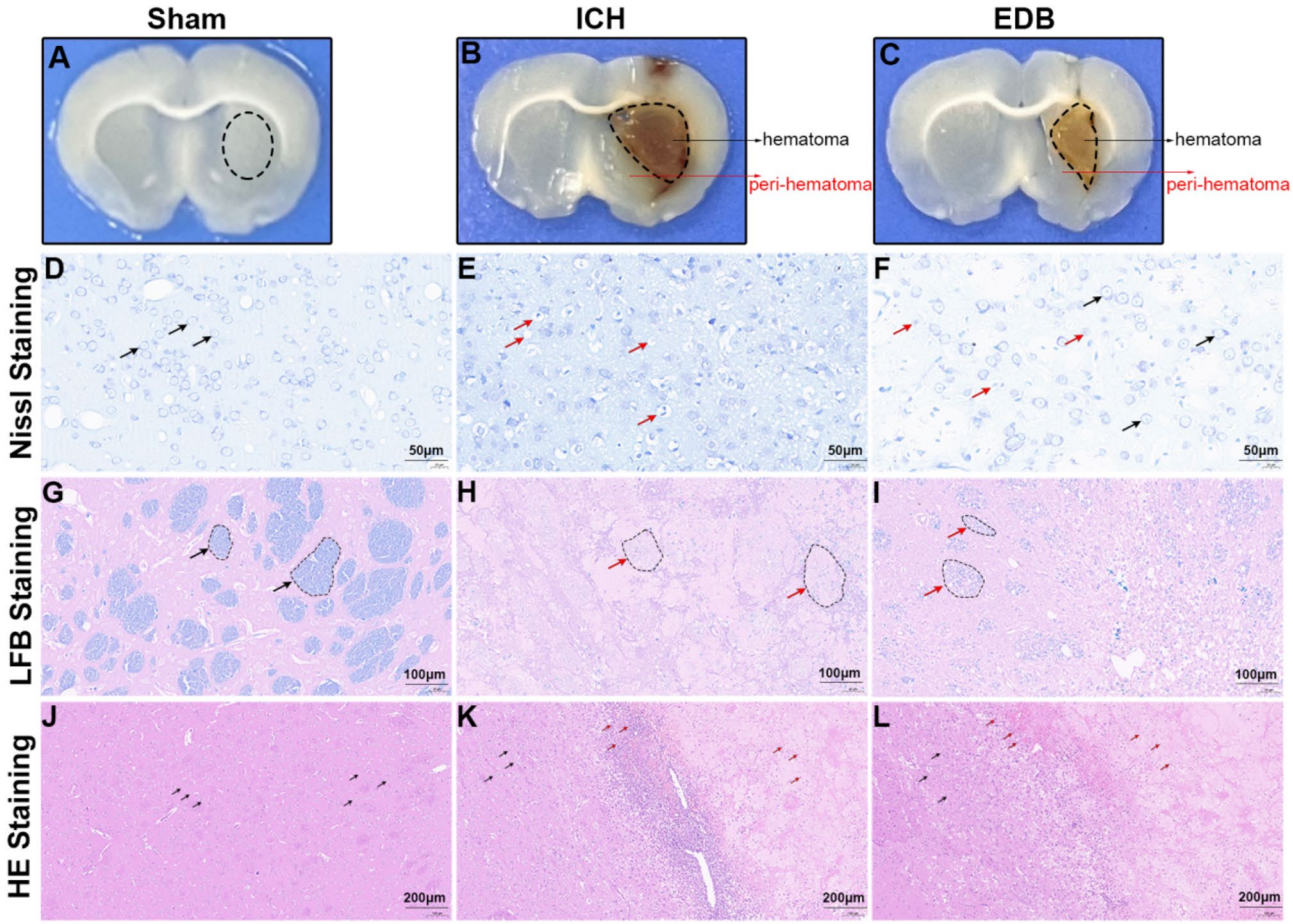

Fig. 2. Detection of pathological injury and inflammation infiltration by Nissl, LFB and HE staining. (**A**–**C**) Representative whole brain slices of different groups with 1 mm thickness. The striatal area demarcated by black oval outlines in (**A**) was used for Nissl staining, HE staining, and LFB staining; The peri-hematomal regions (0.5 mm from the hematoma border) indicated by arrows in (**B**,**C**) were selected for Nissl and HE staining, while the core hematoma areas outlined by black ovals were utilized for LFB staining. (**D**–**F**) Representative Nissl staining images in the perihematomal region of different groups. Black arrow showed normal neurons, while red arrow showed abnormal neurons. (**G**–**I**) Representative LFB staining images in the hematomal region of different groups. Black arrow showed normal myelin plaque, while red arrow showed abnormal myelin plaque. (**J**–**L**) Representative HE staining images in the perihematomal region of different groups. Black arrow showed healthy neurons, while red arrow showed infiltrated inflammatory cells. Scale bar is 50 μm in (**D**–**F**), 100 μm in (**G**–**I**), and 200 μm in (**J**–**L**).

recovery. Nonetheless, the EDB intervention was found to be more effective in reducing lateral ventricle volume compared to the ICH group.

Furthermore, we acquired standard macroscopic images of rat brain anatomy, revealing a significant reduction in hematoma volume in the EDB group compared to the ICH group 3 days post-cerebral hemorrhage (Fig. 3H,I), in alignment with MRI findings.

Edaravone dexborneol alleviated BBB dysfunction of ICH rats

To investigate the impact of EDB on BBB integrity following ICH, the permeability of the microvascular endothelial barrier was assessed by measuring the extravasation of evans blue. In the ICH group, there was a significant increase in evans blue extravasation compared to the Sham group. However, this leakage was mitigated by the administration of EDB (Fig. 4A,C). We also analyzed the protein levels of occludin, ZO-1 and MMP-9 by WB, which played crucial roles in BBB integrity. Our findings revealed that in the ICH group, occludin and ZO-1 protein expression were substantially reduced compared to the Sham group, while MMP-9 level was significantly elevated. Treatment with EDB resulted in a reversal of these effects (Fig. 4B,D–F). These results demonstrate the protective effects of EDB in mitigating BBB disruption in ICH.

Differential expression genes and pathway enrichment analysis

High-throughput mRNA sequencing was utilized to analyze the mRNA expression profiles of striatal tissue samples from rats in the Sham, ICH, and EDB groups. A volcano plot revealed 1532 up-regulated genes and

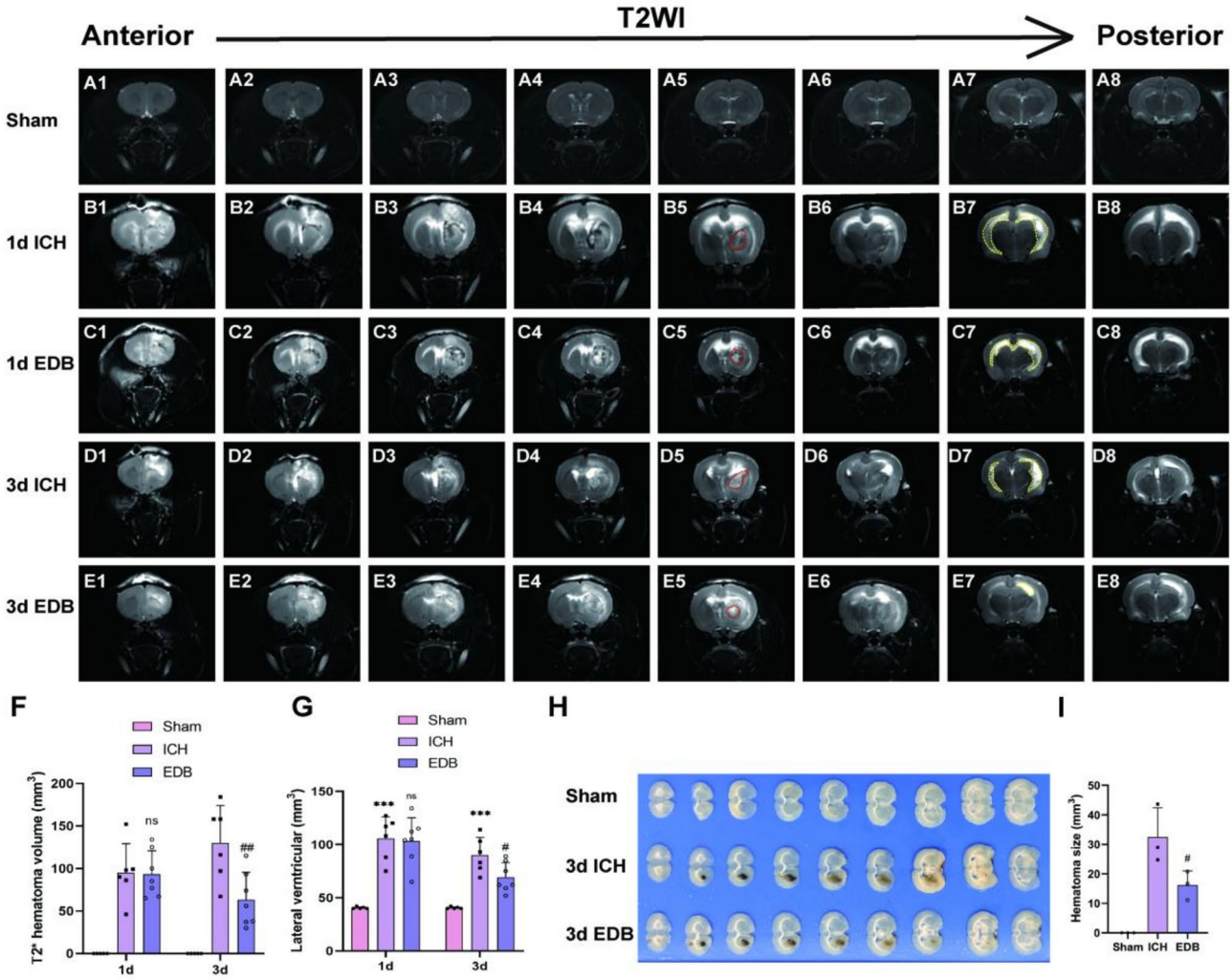

Fig. 3. Detection of hematoma volume and lateral ventricle volume by MRI and tissue section. (**A**–**E**) T2-weighted MRI scans (coronal plane) showing hematoma changes at 1 day and 3 days after ICH. Red dashed lines indicate hematoma size and yellow blood lines indicate lateral ventricle volume. (**F**) Quantitative analysis of hematoma volume on T2WI images at 1 day and 3 days after ICH. (**G**) Quantitative analysis of lateral ventricle volume on T2WI images at 1 day and 3 days after ICH. All data were expressed as mean ± SD. (**H**) Macroscopic images of rat brains (0.5 mm thick) obtained by dissection. (**I**) Quantitative analysis of hematoma volume in brain tissue sections. All data were expressed as mean ± SD. $^{***}P < 0.001$ vs. Sham group; $^{ns}P > 0.05$ vs. ICH group; $^{\#}P < 0.05$ vs. ICH group; $^{\#\#}P < 0.01$ vs. ICH group.

1319 down-regulated genes in the Sham vs. ICH group (Fig. 5A), as well as 466 up-regulated genes and 686 down-regulated genes in the ICH vs. EDB group (Fig. 5B). The comparison of differentially expressed genes (DEGs) between the Sham and ICH groups, and between the ICH and EDB groups, identified 648 unique genes, as depicted in the Venn diagram (Fig. 5C). The 648 unique genes were presented in a heatmap (Fig. 5D). These genes were then analyzed for enrichment using Gene Ontology (GO) and Kyoto Encyclopedia of Genes and Genomes (KEGG) through the "clusterProfiler" package in R software. The GO analysis revealed enrichment in biological processes such as immune response-regulating signaling pathway, neuron death, toll-like receptor signaling pathway, positive regulation of reactive oxygen species metabolic process, glial cell activation, and apoptotic cell clearance (Fig. 5E), as well as in cellular component categories like external side of plasma membrane, lysosome, chromosomal region, etc. (Fig. 5E). Additionally, molecular function categories such as cell adhesion molecule binding, integrin binding, immune receptor activity, phosphoprotein binding, etc. were enriched (Fig. 5E). KEGG analysis indicated the involvement of the differential genes in pathways such as Pl3K-Akt signaling pathway, Rap1 signaling pathway, MAPK signaling pathway, Efferocytosis, Apoptosis, p53 signaling pathway, JAK-STAT signaling pathway, TNF signaling pathway, NF-kappa B signaling pathway, and ferroptosis (Fig. 5F).

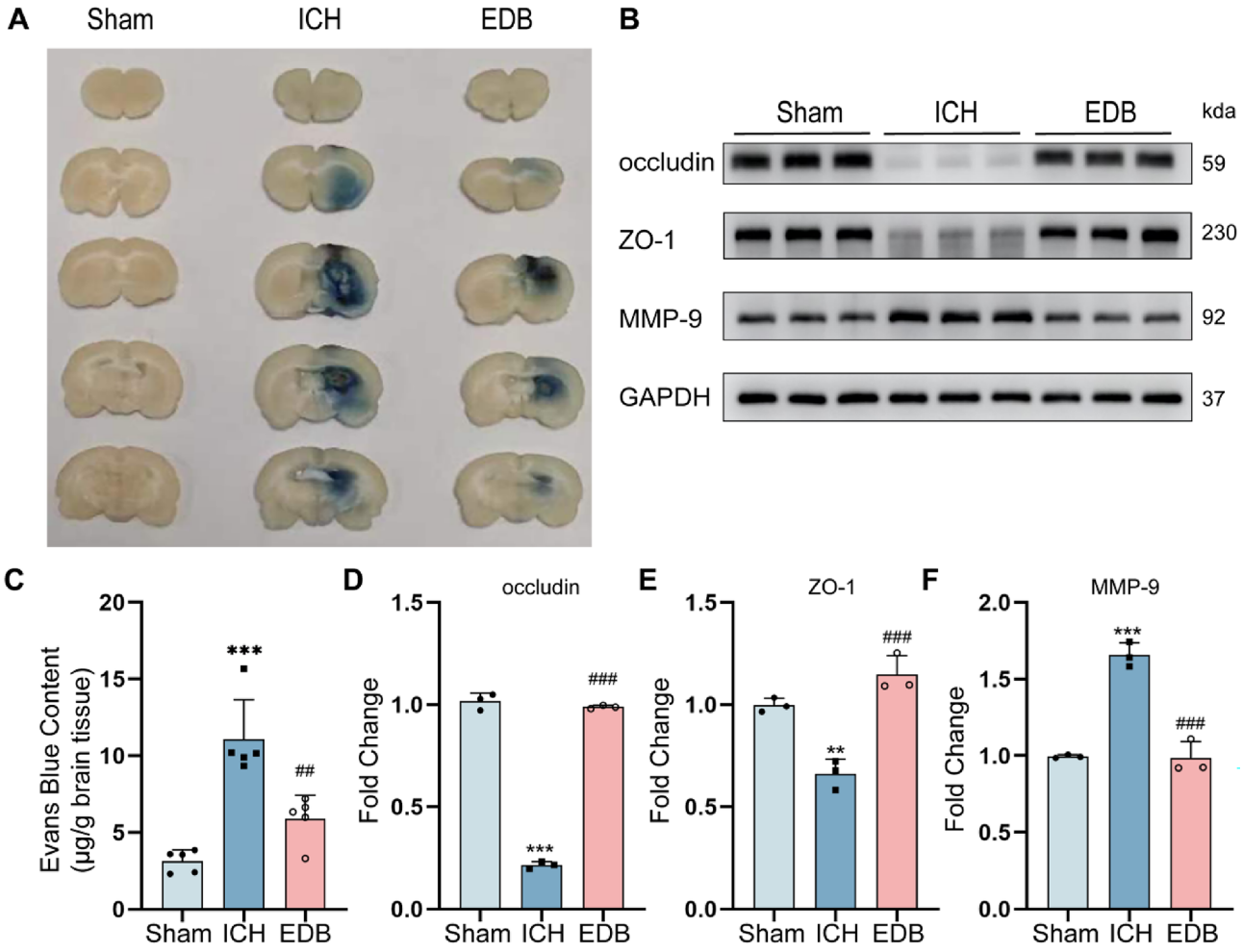

Fig. 4. Detection of BBB integrity by Evans blue staining and WB. (**A**) Representative images showing Evans blue extravasation 3 days after ICH induction. (**B**) Representative western blot images of occludin, ZO-1 and MMP-9 in striatum brain tissue of rat brain. Occludin belt was cropped between 50 and 70 kDa. ZO-1 belt was cropped between 150 and 250 kDa. MMP-9 belt was cropped between 70 and 100 kDa. GAPDH belt was cropped between 35 and 40 kDa. ZO-1 and GAPDH were cropped from the same gel, while Occludin and MMP-9 were cropped from different gels. Full-length blots were presented in Additional file 1: Fig. S1A–D. (**C**) Quantification of Evans blue content in the right brain hemisphere of rats. (**D**–**F**) Quantification of western blot results of occludin, ZO-1 and MMP-9. $^{**}P < 0.01$ vs. Sham group; $^{***}P < 0.001$ vs. Sham group; $^{\#\#}P < 0.01$ vs. ICH group; $^{\#\#\#}P < 0.001$ vs. ICH group. All data were expressed as mean ± SD of 5 rats.

Edaravone dexborneol attenuated ICH by inhibiting ferroptosis

To validate the potential of EDB in ameliorating ICH through the inhibition of ferroptosis, as indicated by the results of KEGG analysis, various ferroptosis markers including Fe^{2+}, 4-HNE, MDA, GSH, and T-SOD were assessed at day 3, and a range of proteins associated with ferroptosis signaling pathways were assessed at day3 and day 7. The results of Prussian blue staining indicated a notable accumulation of iron around the hematoma in rats of ICH group and the administration of EDB markedly diminished the extent of iron deposition (Fig. 6A–C). Correspondingly, the levels of Fe^{2+} in the striatum tissue were significantly heightened in ICH rats compared to those in the Sham group, with EDB treatment effectively mitigating the rise in Fe^{2+} concentration (Fig. 6D). Lipid peroxidation and oxidative stress are critical mechanisms in the pathogenesis of ferroptosis. As demonstrated in Fig. 6E–H, the levels of 4-HNE and MDA were notably elevated, while the levels of GSH and T-SOD were significantly reduced in the striatum tissue of ICH rats compared to those in the Sham group. These alterations were effectively reversed by treatment with EDB. Furthermore, the western blot results indicated a significant decrease in the protein expression of GPX4, NRF2, SLC7A11, HIF1α, and HMOX-1 in the ICH group compared to the Sham group both on day3 and day 7. Treatment with EDB demonstrated a reversal of this trend, as depicted in Fig. 6I,J. It's worth to mention that the expression level of P53 also greatly changed in the ICH and EDB group, which indicated P53 pathway may involved in the ferroptosis progression. Thus, it is postulated that the therapeutic efficacy of EDB in treating ICH may be attributed, at least in part, to its inhibition of ferroptosis.

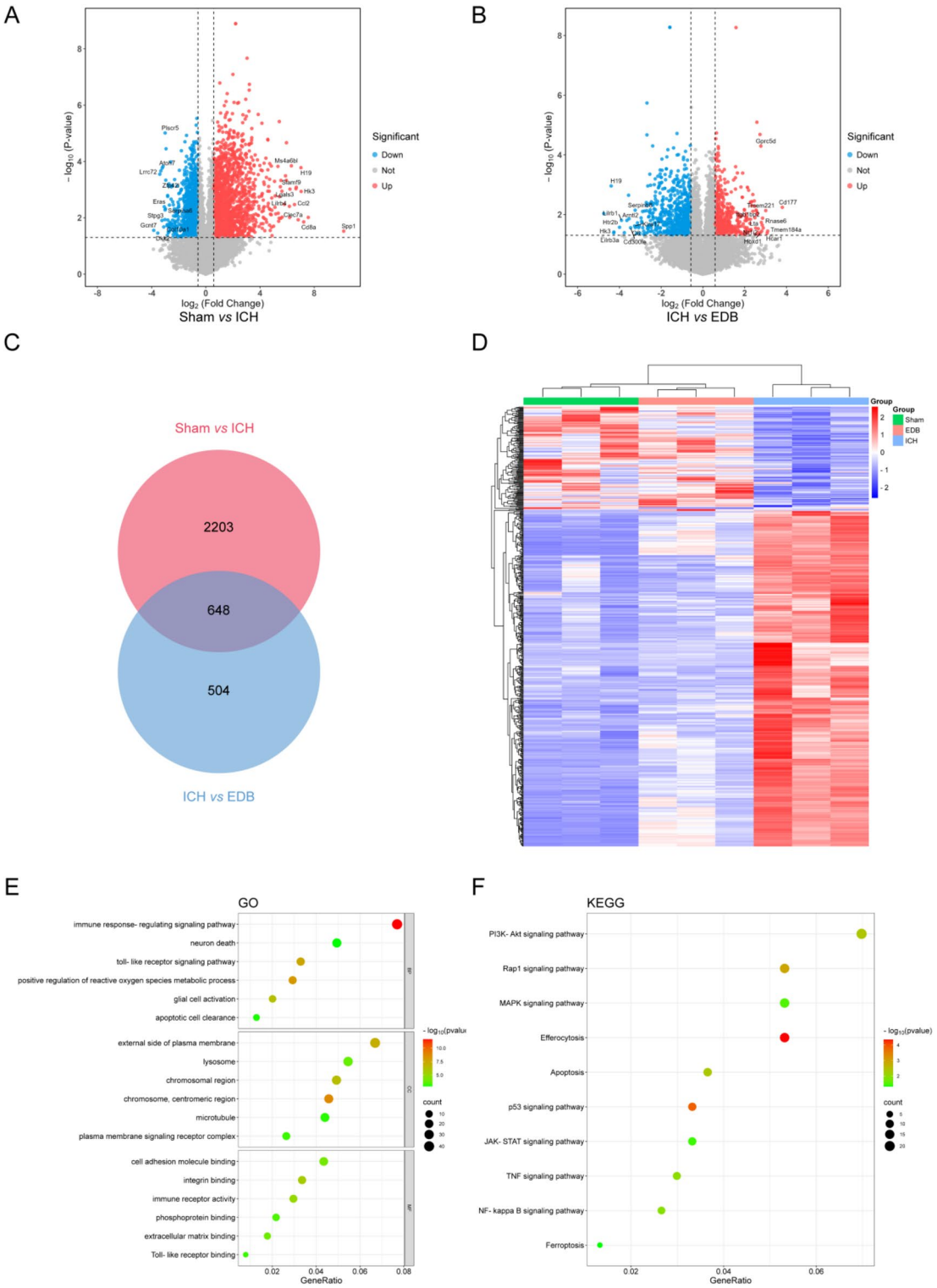

Fig. 5. Differential expression genes and pathway enrichment analysis. (**A**) Volcano plot displayed DEGs between Sham and ICH. (**B**) Volcano plot displayed DEGs between ICH and EDB. (**C**) Venn diagram showed the common DEGs between Sham vs. ICH and ICH vs. EDB. (**D**) Heatmap demonstrated the 684 unique genes. (**E**) Gene ontology biological processes (GO-BP), cellular component (GO-CC) and molecular functions (GO-MF). (**F**) KEGG enrichment analysis[21] showed signaling pathway that the DEGs involved in.

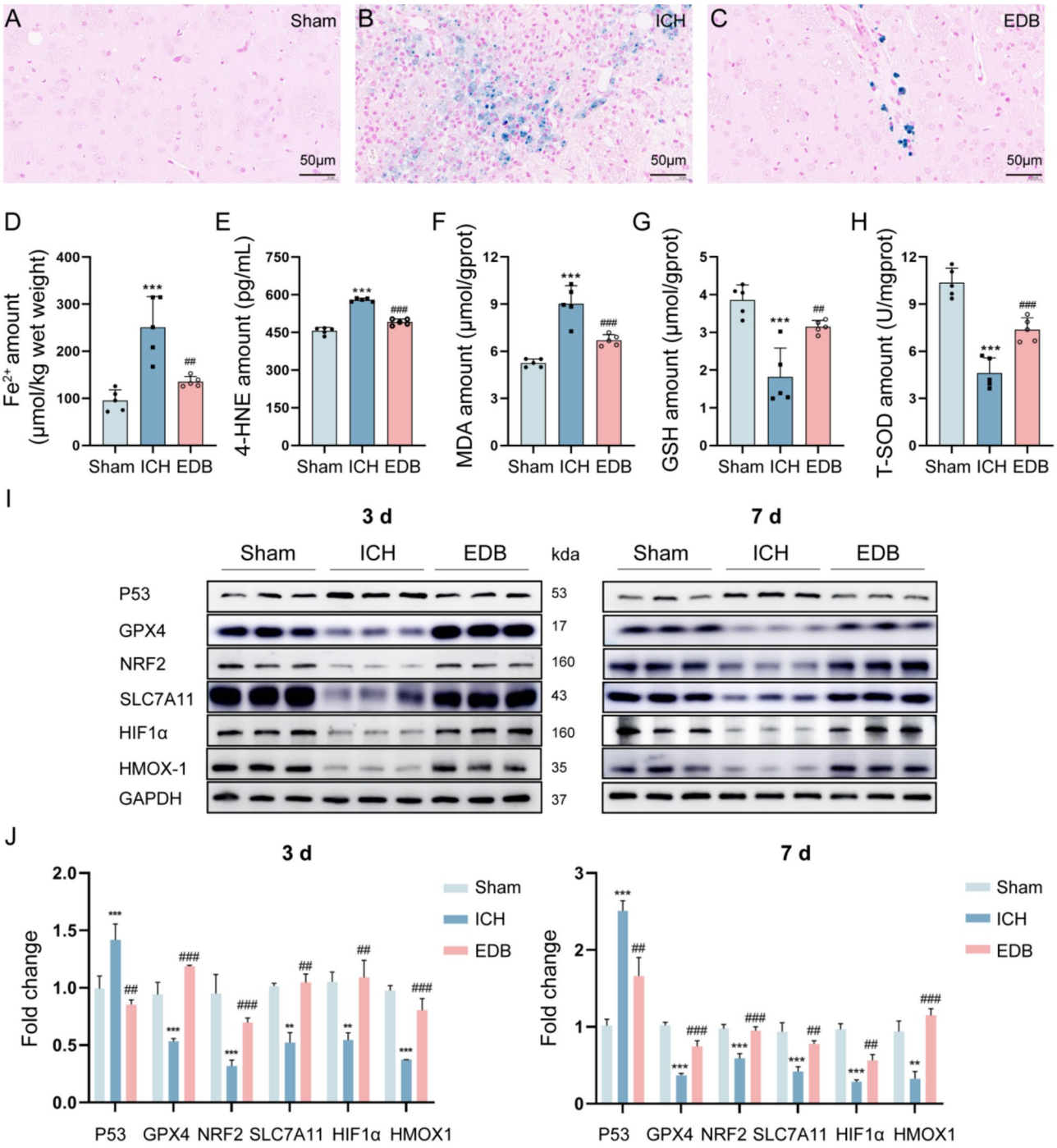

Fig. 6. Detection of ferroptosis-related markers. (**A**–**C**) Brain sections were subjected to Prussian blue staining to detect the deposition of iron in the perihematoma of brain tissues, Bar = 200 μm. (**D**–**H**) The content of Fe^{2+}, 4-HNE, MDA, GSH, and T-SOD in the striatum tissue of rats were detected. (**I**) Representative western blot images of P53, GPX4, NRF2, SLC7A11, HIF1α, and HMOX1 at day 3 and day 7. P53 belt was cropped between 50 and 70 kDa. GPX4 belt was cropped between 17 and 25 kDa. NRF2 belt was cropped between 150 and 250 kDa. SLC7A11 belt was cropped between 40 and 50 kDa. HIF1α belt was cropped between 150 and 250 kDa. HMOX1 belt was cropped between 35 and 40 kDa. GAPDH belt was cropped between 35 and 40 kDa. On Day 3, the HMOX1 and HIF1α belts were cropped from the same gel, while other belts were cropped from different gels. On Day 7, the NRF2 and GPX4 belts were cropped from the same gel, while other bands were cropped from different gels. Full-length blots were presented in Additional file 2: Fig. S2A–M. (**J**) Quantification of protein expression levels of WB bands in Figure (**I**). $^{**}P < 0.01$ vs. Sham group; $^{***}P < 0.001$ vs. Sham group; $^{\#\#}P < 0.01$ vs. ICH group; $^{\#\#\#}P < 0.001$ vs. ICH group. All data were expressed as mean ± SD of 5 rats.

Fer-1 synergisticly increases the inhibition of ferroptosis after cerebral hemorrhage by edaravone dexborneol

To further explore the relationship between EDB and ferroptosis, Fer-1, an inhibitor of ferroptosis, was used as a positive control. We evaluated various ferroptosis markers, including Fe^{2+}, MDA, GSH, T-SOD, and a series of proteins associated with the ferroptosis signaling pathway. As illustrated in Fig. 7A–D, the concentrations of MDA and Fe^{2+} were markedly reduced, whereas the levels of GSH and T-SOD were significantly elevated in the striatum tissues of rats in the Fer-1 and EDB groups compared to those in the ICH group. Additionally, our findings indicated that MDA and Fe^{2+} levels were further decreased in the Fer-1 + EDB group relative to the Fer-1 and EDB groups. Conversely, GSH and T-SOD levels were higher in the Fer-1 + EDB group than those in the Fer-1 and EDB groups. Western blot analysis revealed a significant reduction in the protein expression of P53, whereas the protein expression levels of GPX4, NRF2, SLC7A11, HIF1α, and HMOX-1 were significantly elevated in the Fer-1, EDB, and Fer-1 + EDB groups compared to the ICH group (Fig. 7E–K). Notably, the expression level of P53 in the Fer-1 + EDB group was lower than that in the Fer-1 and EDB groups, while the expression level of SLC7A11 in the Fer-1 + EDB group was higher than that in the Fer-1 and EDB groups. Collectively, these in vivo results suggest that both Fer-1 and EDB may exert protective effects in the progression of ICH by inhibiting ferroptosis. Moreover, Fer-1 may have synergistic inhibitory effect of EDB on ferroptosis after cerebral hemorrhage.

EDB protects against ferroptosis via regulation P53/GPX4 signaling pathway

To investigate the hypothesis that EDB-mediated inhibition of ferroptosis in ICH is facilitated through the P53/GPX4 signaling pathway, PC-12 cells were exposed to hemin to establish an in vitro ICH model and subsequently treated with EDB, PFTα (a P53 inhibitor), or a combination of EDB and PFTα. The cell viability assay revealed that the reduction in PC-12 cell viability induced by hemin exposure was partially ameliorated by treatment with EDB, PFTα, or the combination of EDB and PFTα (Fig. 8A). Furthermore, the results from 4-HNE detection and C11-BODIPY staining demonstrated that treatment with PFTα alone significantly decreased the levels of peroxides in PC-12 cells, mirroring the effects observed with EDB treatment (Fig. 8B–D). Furthermore, western blot results demonstrated a reduction in P53 expression levels in the EDB, PFTα, and EDB + PFTα groups compared to the hemin group, while the protein expression level of GPX4 was significantly elevated (Fig. 8E–G). These findings suggest that EDB confers a protective effect in ICH by modulating the P53/GPX4 signaling pathway. A graphical summary of this study was shown in Fig. 8H.

Discussion

To elucidate the protective mechanisms of EDB in cerebral hemorrhage, we conducted RNA sequencing and bioinformatics analyses on striatal tissue three days post-hemorrhage onset. GO analysis revealed that "positive regulation of reactive oxygen species metabolic process" was among the top five most enriched biological processes. Additionally, "ferroptosis" emerged as one of the top ten enriched signaling pathways in the KEGG analysis. Furthermore, our findings indicate that both EDB and Fer-1 consistently regulate the expression of ferroptosis-related proteins. Notably, the combined treatment group (Fer-1 + EDB) exhibited a more pronounced inhibitory effect on certain ferroptosis-related proteins and oxidative stress factors compared to the individual Fer-1 and EDB groups. This suggests that EDB significantly ameliorates cerebral hemorrhage injury through regulating ferroptosis. Moreover, the data imply a potential synergistic interaction between Fer-1 and EDB in the inhibition of ferroptosis.

The tumor suppressor protein P53 emerges as a pivotal regulator of various cellular processes, including proliferation, senescence, and apoptosis[22]. Recent studies have increasingly substantiated the close association between the P53 protein and the metabolic pathways involved in ferroptosis[23]. P53 plays a bifunctional role in the regulation of ferroptosis, capable of both promoting and inhibiting this form of cell death[23]. When lipid peroxidation damage is minimal and reparable, P53 facilitates the suppression of ferroptosis, aiding in cellular recovery. Conversely, in instances where the damage is extensive or irreparable, P53 triggers ferroptosis, leading to the elimination of compromised cells. The regulatory mechanisms of ferroptosis by P53 are categorized into canonical and noncanonical pathways, based on their dependence on GPX4[23]. In the noncanonical pathway, P53 modulates ferroptosis via the arachidonate 12-lipoxygenase (ALOX12)[24], arachidonate lipoxygenase 3 (ALOXE3)[25], or iPLA2β pathway[26]. The canonical pathway of P53 that regulates ferroptosis involves the metabolism of iron, lipids, amino acids and ROS[27]. P53 directly targets the responsive element in the promoter region of SLC7A11 to suppress its expression, consequently increasing cellular susceptibility to ferroptosis. As the uptake of extracellular cystine decreases, the synthesis of glutathione (GSH) diminishes, leading to reduced activity of GPX4, an accumulation of lipid peroxides, and ultimately, the induction of ferroptosis[28]. Additionally, P53 inhibits the serine transsulfuration pathway by repressing cystathionine β-synthase. This limits the production of GSH and thereby indirectly inhibits the enzymatic activity of GPX4, eventually promoting ferroptosis[29]. In this study, the "P53 signaling pathway" was identified as one of the ten signaling pathways with the highest KEGG enrichment. The expression level of P53 was significantly reduced following treatment with EDB or Fer-1, suggesting that the P53 pathway is implicated in the mechanism by which EDB inhibits ferroptosis. Furthermore, in vitro experiments demonstrated that the P53 inhibitor PFT-α significantly upregulated the expression of SLC7A11 and GPX4 while concurrently downregulating P53 expression. Based on these findings, we hypothesize that EDB may mitigate ferroptosis and ameliorate cerebral hemorrhage injury by modulating the P53/SLC7A11/GPX4 signaling pathway.

While the mechanistic link between EDB and ferroptosis upstream regulators remains unclear in the specific context of ICH, emerging evidence from related neurological conditions might provide valuable mechanistic clues. Notably, recent studies in cerebral ischemia and depression models have demonstrated that EDB and its main component edaravone exert therapeutic effects through ferroptosis regulation. Xiao et al.. reported

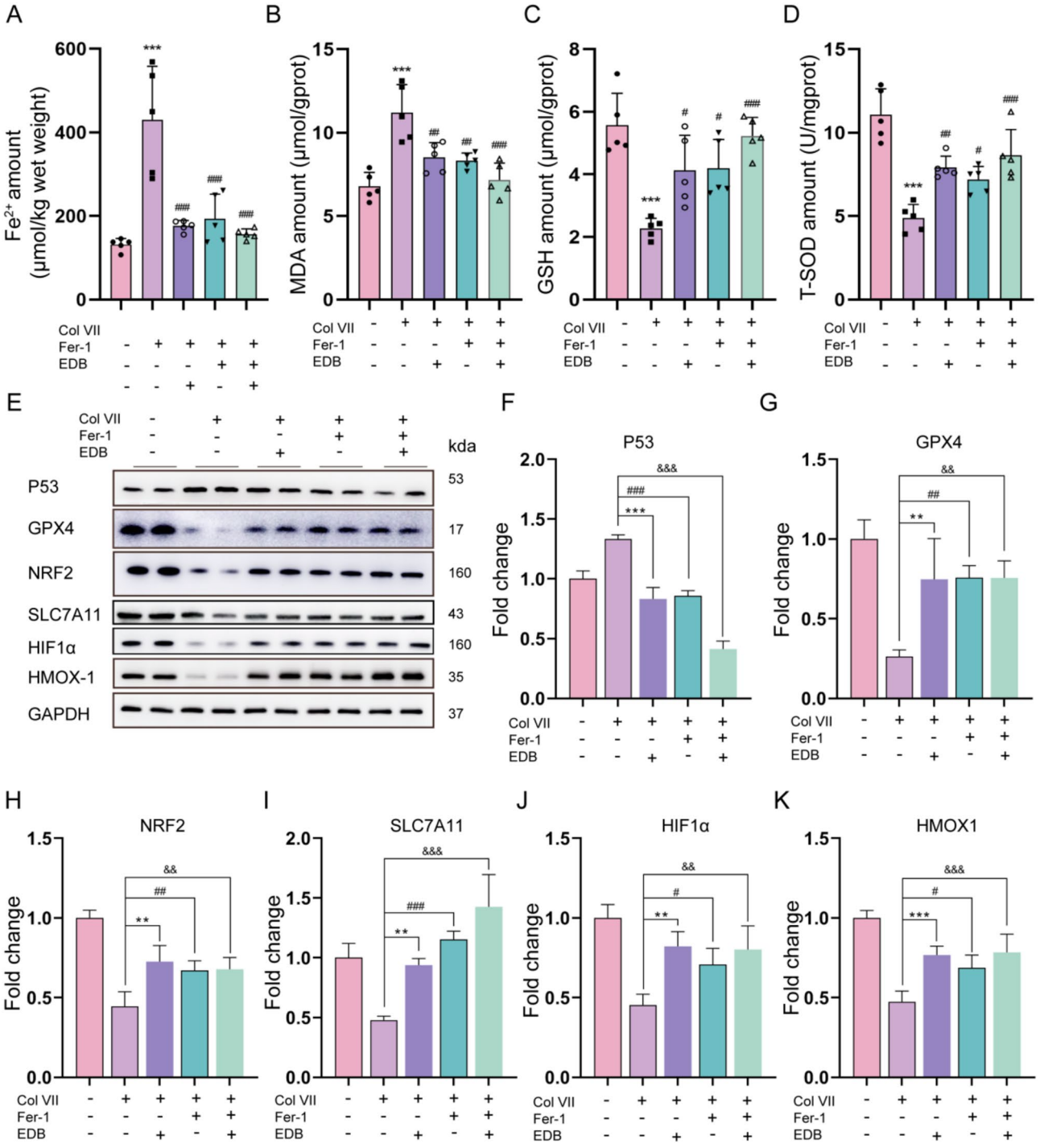

Fig. 7. Analysis of ferroptosis-related markers. (**A**–**D**) The content of Fe^{2+}, MDA, GSH, and T-SOD in the striatum tissue of rats was detected. $^{**}P<0.01$ vs. Sham group; $^{***}P<0.001$ vs. Sham group; $^{\#}P<0.05$ vs. ICH group; $^{\#\#}P<0.01$ vs. ICH group; $^{\#\#\#}P<0.001$ vs. ICH group. (**E**) Representative western blot images of P53, GPX4, NRF2, SLC7A11, HIF-1α and HMOX-1. P53 belt was cropped between 50 and 70 kDa. GPX4 belt was cropped between 17 and 25 kDa. NRF2 belt was cropped between 150 and 250 kDa. SLC7A11 belt was cropped between 40 and 50 kDa. HIF1α belt was cropped between 150 and 250 kDa. HMOX1 belt was cropped between 35 and 40 kDa. GAPDH belt was cropped between 35 and 40 kDa. P53 and GAPDH belts were cropped from the same gel, while the other blots were cropped from different gels. Full-length blots were presented in Additional file 3: Fig. S3A–G. (**F**–**K**) Quantification of western blot results of P53, GPX4, NRF2, SLC7A11, HIF-1α and HMOX-1. $^{**}P<0.01$ vs. ICH group; $^{***}P<0.001$ vs. ICH group; $^{\#}P<0.05$ vs. ICH group; $^{\#\#}P<0.01$ vs. ICH group; $^{\#\#\#}P<0.001$ vs. ICH group. $^{\&\&}P<0.01$ vs. ICH group; $^{\&\&\&}P<0.001$ vs. ICH group. All data were expressed as mean ± SD of 5 rats.

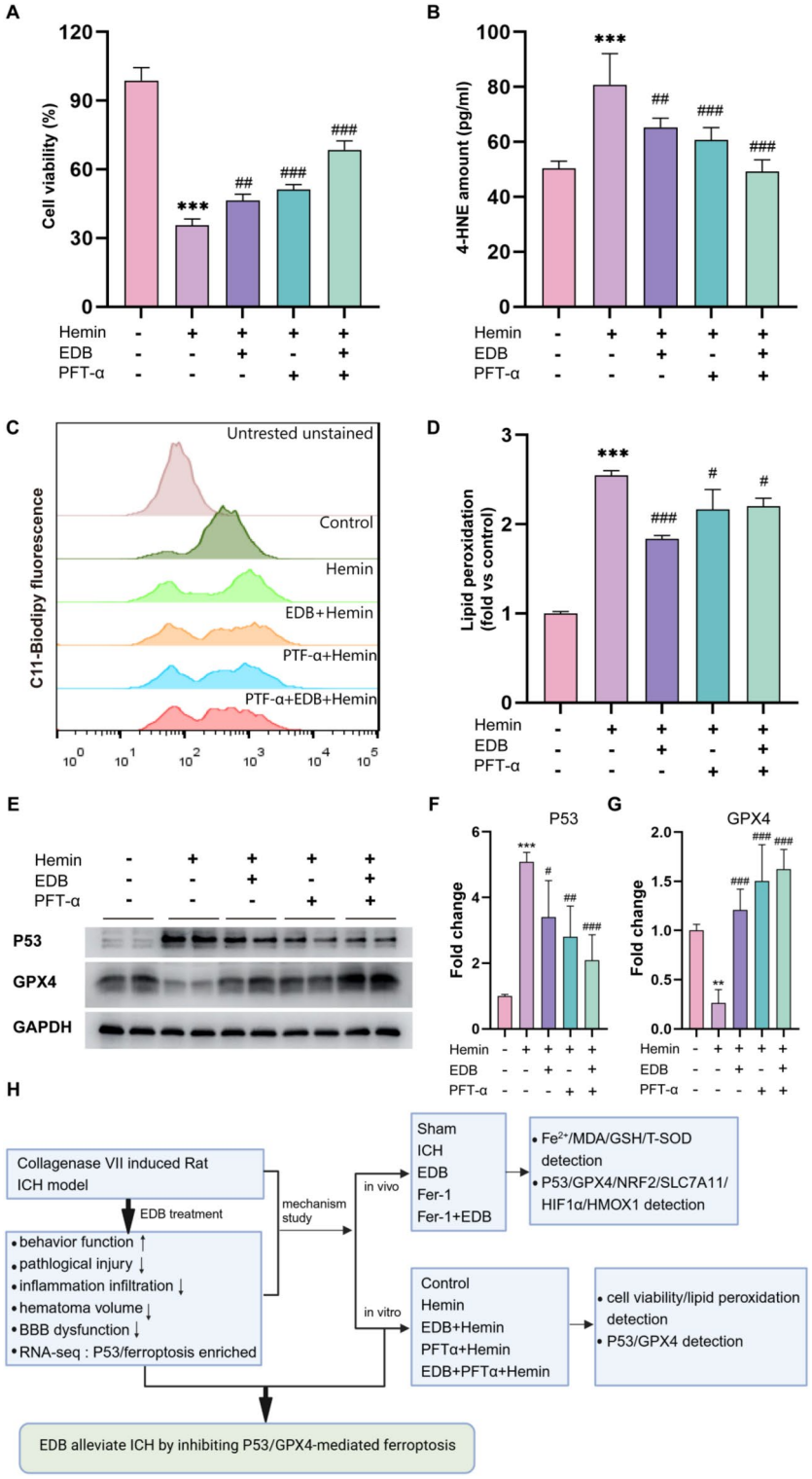

Fig. 8. Detection of ferroptosis-related markers in vitro. (**A**) Cell viability was detected by CCK-8 assay. (**B**) The level of 4-HNE in PC12 cells was detected by ELISA. (**C**) Representative flow cytometry histogram of C11 BODIPY fluorescence in PC12 cells. (**D**) Quantification of flow cytometry results described in (**C**). (**E**) Representative western blot bands of P53, GPX4. P53 belt was cropped between 50 and 70 kDa. GPX4 belt was cropped between 15 and 20 kDa. GAPDH belt was cropped between 35 and 40 kDa. All belts were cropped from different gels. Full-length blots were presented in Additional file 4: Fig. S4A–C. (**F**,**G**) Quantification of western blot results of P53 and GPX4. (**H**) Graphical summary of this study. All data were expressed as the mean ± SD. $^{**}P < 0.01$ vs. Sham group; $^{***}P < 0.001$ vs. Sham group; $^{\#}P < 0.05$ vs. ICH group; $^{\#\#}P < 0.01$ vs. ICH group; $^{\#\#\#}P < 0.001$ vs. ICH group.

that EDB protects against cerebral ischemia/reperfusion injury by suppressing ferroptosis through activation of the NRF2/HMOX1/GPX4 signaling axis[30]. Similarly, Liu et al. identified that edaravone ameliorates cerebral ischemic injury by modulating the NRF2/ferroportin pathway[31]. Furthermore, Dang et al.. revealed that edaravone improves depressive behaviors via the SIRT1/NRF2/HMOX1/GPX4 cascade[32]. These findings collectively suggest that EDB or edaravone-mediated neuroprotection may share conserved regulatory mechanisms across different neurological pathologies. In our ICH model, we observed that EDB treatment significantly rescued the decreased expression of both NRF2 and HMOX1 (Fig. 6I). This consistent pattern with previous reports in ischemic and depressive models implies that the NRF2/HMOX1 axis might serve as a critical pathway for EDB's anti-ferroptotic effects in ICH. Further studies will perform gain-of-function (e.g., NRF2/HMOX1 overexpression) and loss-of-function (e.g., siRNA knockdown or CRISPR/Cas9-mediated gene editing) experiments to comprehensively characterize EDB's regulatory network in ICH-associated ferroptosis.

Hypoxia-inducible factor-1α (HIF1α) is a subunit of hypoxia-inducible factor-1 (HIF1) that primarily functions to regulate gene expression under hypoxic conditions, thereby facilitating cellular adaptation to hypoxia[33,34]. Moreover, HIF1α has been implicated in the regulation of ferroptosis across various diseases, with its role varying under different pathological conditions. For example, the HIF1α/HO-1 pathway has been demonstrated to promote ferroptosis in lung injury and testicular injury[35,36]. Conversely, in the contexts of atherosclerosis and hyperlipidemia, the activation of HIF1α has been shown to inhibit ferroptosis, improved mitochondrial function and lipid metabolism[37]. Yuan et al.. reported that sorafenib attenuates liver fibrosis by inducing hepatic stellate cell ferroptosis via the HIF1α/SLC7A11 pathway[38]. Additionally, HIF1α has been shown to ameliorate brain injury following ischemic stroke by inhibiting ferroptosis through the downregulation of ACSL4[39]. In our study, we observed a reduction in HIF1α protein levels following the onset of ICH. Treatment with EDB or Fer-1 significantly upregulated the expression of HIF1α, suggesting a protective role for HIF1α in ICH pathology. The two-sided role of HIF1α in ferroptosis regulation may be related to its different downstream genes targeted in different diseases. It's necessary to further investigate the complex and important role of HIF1α in ICH.

Tight junction proteins, such as ZO-1 and occludin, are integral to the maintenance of the blood-brain barrier (BBB) structure and function[40]. Occludin, a transmembrane tight junction protein, is crucial for both the barrier function of tight junctions and their signal transduction processes[41]. ZO-1, a member of the membrane-associated guanylate kinase (MAGUK) family, is essential for preserving cellular structural integrity and normal polarity, as well as playing a significant role in cell connectivity and signal transduction. ZO-1 is intimately associated with other tight junction components, such as occludin, through its PDZ domain. Damage to ZO-1 results in altered tight junction functionality, rendering ZO-1 a critical biomarker for assessing the barrier integrity and permeability of various tissues[40]. As a significant protease within the matrix metalloproteinases (MMPs) family, MMP-9 has been demonstrated to compromise the BBB by degrading the capillary basement membrane and tight junction proteins[42,43]. Our findings indicated that the expression levels of ZO-1 and occludin were elevated, whereas MMP-9 levels were decreased following EDB treatment in comparison to the ICH group. Additionally, we evaluated the permeability of BBB by measuring Evans blue extravasation and observed a significant reduction in Evans blue leakage in the EDB-treated group. These results underscore the protective role of EDB in restoring BBB integrity. Furthermore, our KEGG analysis revealed that DEGs are enriched in the Rap1 signaling pathway. Rap1 signaling pathway has not only been shown to enhance intercellular tight junctions in vitro, but has also been shown to ameliorate MCAO-induced BBB damage in vivo[44]. Based on these observations, we hypothesize that EDB may mitigate BBB disruption in an ICH rat model through the activation of the Rap1 pathway. More experiments need to be designed to test this hypothesis.

It is necessary to acknowledge the limitations of this work. In this study, considering hormonal confounders[45] and field-specific conventions[46], male rats were used as experimental subjects. We recognize that this design limits the generalizability of our results to female populations and precludes insights into sex-specific pathophysiology. To mitigate these limitations, parallel experiments will be performed to compare male and female SD rats in the same ICH model. While recognizing the limitations of single-sex models, this approach aligns with current norms in translational stroke research to minimize confounding variables during initial mechanistic exploration. We believe this approach lays a critical foundation for subsequent sex-disaggregated research. Our current study focused exclusively on 7-day post-ICH outcomes, which represents a limitation in comprehensively evaluating EDB's sustained therapeutic effects. We propose to implement extended observation windows (up to 28–56 days post-ICH) in subsequent investigations, incorporating both functional assessments (e.g., mNSS, rotarod, Morris water maze) and histopathological evaluations at multiple chronic timepoints. This systematic approach will help elucidate temporal patterns of neuroprotection and establish optimal therapeutic windows for EDB administration.This study exclusively assessed the protective effects of EDB on cerebral hemorrhage through the regulation of ferroptosis, without exploring other potential mechanisms. Notably, KEGG analysis revealed enrichment in the PI3K-Akt, MAPK, JAK-STAT, and NF-κB signaling pathways, which are associated with apoptosis and inflammation. Whether EDB alleviates ICH outcome through these pathways remain to be further studied. Furthermore, while we observed the accumulation of inflammatory cells around the hematoma post-intracerebral hemorrhage, we did not differentiate between cell types or investigate the related migration mechanisms. Besides, the specific cell types on which EDB exerts its effects following intracerebral hemorrhage remain to be elucidated.

Data availability

The datasets generated and analysed during the current study are available in the Gene Expression Omnibus repository, Accession number: GSE288102.

Received: 24 January 2025; Accepted: 17 April 2025

Published online: 13 May 2025

References

1. Keep, R. F., Hua, Y. & Xi, G. Intracerebral haemorrhage: mechanisms of injury and therapeutic targets. *Lancet Neurol.* **11**, 720–731. https://doi.org/10.1016/s1474-4422(12)70104-7 (2012).
2. Manaenko, A. et al. Inhibition of stress fiber formation preserves blood-brain barrier after intracerebral hemorrhage in mice. *J. Cereb. Blood Flow. Metab.* **38**, 87–102. https://doi.org/10.1177/0271678x16679169 (2018).
3. Zhao, L. et al. Recombinant CTRP9 administration attenuates neuroinflammation via activating adiponectin receptor 1 after intracerebral hemorrhage in mice. *J. Neuroinflamm.* **15**, 215. https://doi.org/10.1186/s12974-018-1256-8 (2018).
4. Zhu, H. et al. Role and mechanisms of cytokines in the secondary brain injury after intracerebral hemorrhage. *Prog. Neurobiol.* **178**, 101610. https://doi.org/10.1016/j.pneurobio.2019.03.003 (2019).
5. Li, Q. et al. Inhibition of neuronal ferroptosis protects hemorrhagic brain. *JCI Insight.* **2**, e90777. https://doi.org/10.1172/jci.insight.90777 (2017).
6. Zille, M. et al. Neuronal death after hemorrhagic stroke in vitro and in vivo shares features of ferroptosis and necroptosis. *Stroke* **48**, 1033–1043. https://doi.org/10.1161/strokeaha.116.015609 (2017).
7. Fung, C. et al. Effect of decompressive craniectomy on perihematomal edema in patients with intracerebral hemorrhage. *PLoS One.* **11**, e0149169. https://doi.org/10.1371/journal.pone.0149169 (2016).
8. Chen, W. et al. Inhibition of mitochondrial ROS by MitoQ alleviates white matter injury and improves outcomes after intracerebral haemorrhage in mice. *Oxid. Med. Cell. Longev.* **2020** (8285065). https://doi.org/10.1155/2020/8285065 (2020).
9. Gozzelino, R., Jeney, V. & Soares, M. P. Mechanisms of cell protection by Heme oxygenase-1. *Annu. Rev. Pharmacol. Toxicol.* **50**, 323–354. https://doi.org/10.1146/annurev.pharmtox.010909.105600 (2010).
10. Wan, J., Ren, H. & Wang, J. Iron toxicity, lipid peroxidation and ferroptosis after intracerebral haemorrhage. *Stroke Vasc. Neurol.* **4**, 93–95. https://doi.org/10.1136/svn-2018-000205 (2019).
11. Liu, T. et al. Bioinformatics analysis identifies potential ferroptosis key genes in the pathogenesis of intracerebral hemorrhage. *Front. Neurosci.* **15**, 661663. https://doi.org/10.3389/fnins.2021.661663 (2021).
12. Rosell, A. et al. Brain perihematoma genomic profile following spontaneous human intracerebral hemorrhage. *PLoS One.* **6**, e16750. https://doi.org/10.1371/journal.pone.0016750 (2011).
13. Zhang, X. et al. (+)-Borneol improves the efficacy of Edaravone against DSS-induced colitis by promoting M2 macrophages polarization via JAK2-STAT3 signaling pathway. *Int. Immunopharmacol.* **53**, 1–10. https://doi.org/10.1016/j.intimp.2017.10.002 (2017).
14. Hu, R. et al. Edaravone dexborneol provides neuroprotective benefits by suppressing NLRP3 inflammasome-induced microglial pyroptosis in experimental ischemic stroke. *Int. Immunopharmacol.* **113**, 109315. https://doi.org/10.1016/j.intimp.2022.109315 (2022).
15. Xu, J. et al. Edaravone dexborneol versus edaravone alone for the treatment of acute ischemic stroke: A phase III, randomized, double-blind, comparative trial. *Stroke.* **52**, 772–780. https://doi.org/10.1161/strokeaha.120.031197 (2021).
16. Chen, Q. et al. Edaravone dexborneol treatment attenuates neuronal apoptosis and improves neurological function by suppressing 4-HNE-associated oxidative stress after subarachnoid hemorrhage. *Front. Pharmacol.* **13**, 848529. https://doi.org/10.3389/fphar.2022.848529 (2022).
17. Johnson, G. A., Calabrese, E., Badea, A., Paxinos, G. & Watson, C. A multidimensional magnetic resonance histology atlas of the Wistar rat brain. *Neuroimage* **62**, 1848–1856. https://doi.org/10.1016/j.neuroimage.2012.05.041 (2012).
18. Li, H. et al. Menstrual blood-derived endometrial stem cells alleviate neuroinflammation by modulating M1/M2 polarization in cell and rat Parkinson's disease models. *Stem Cell. Res. Ther.* **14**, 85. https://doi.org/10.1186/s13287-023-03330-7 (2023).
19. Chen, Q. et al. Simvastatin promotes hematoma absorption and reduces hydrocephalus following intraventricular hemorrhage in part by upregulating CD36. *Transl. Stroke Res.* **8**, 362–373. https://doi.org/10.1007/s12975-017-0521-y (2017).
20. Hou, Y. et al. Oxygen glucose deprivation-pretreated astrocyte-derived exosomes attenuates intracerebral hemorrhage (ICH)-induced BBB disruption through miR-27a-3p /ARHGAP25/Wnt/β-catenin axis. *Fluids Barriers CNS.* **21**, 8. https://doi.org/10.1186/s12987-024-00510-2 (2024).
21. Kanehisa, M., Furumichi, M., Sato, Y., Matsuura, Y. & Ishiguro-Watanabe, M. KEGG: biological systems database as a model of the real world. *Nucleic Acids Res.* **53**, D672–d677. https://doi.org/10.1093/nar/gkae909 (2025).
22. Peuget, S., Zhou, X. & Selivanova, G. Translating p53-based therapies for cancer into the clinic. *Nat. Rev. Cancer.* **24**, 192–215. https://doi.org/10.1038/s41568-023-00658-3 (2024).
23. Xu, R., Wang, W. & Zhang, W. Ferroptosis and the bidirectional regulatory factor p53. *Cell. Death Discov.* **9**, 197. https://doi.org/10.1038/s41420-023-01517-8 (2023).
24. Chu, B. et al. ALOX12 is required for p53-mediated tumour suppression through a distinct ferroptosis pathway. *Nat. Cell. Biol.* **21**, 579–591. https://doi.org/10.1038/s41556-019-0305-6 (2019).
25. Yang, X. et al. miR-18a promotes glioblastoma development by down-regulating ALOXE3-mediated ferroptotic and anti-migration activities. *Oncogenesis* **10**, 15. https://doi.org/10.1038/s41389-021-00304-3 (2021).
26. Malley, K. R. et al. The structure of iPLA(2)β reveals dimeric active sites and suggests mechanisms of regulation and localization. *Nat. Commun.* **9**, 765. https://doi.org/10.1038/s41467-018-03193-0 (2018).
27. Wang, Y. et al. Ferroptosis: underlying mechanisms and involvement in neurodegenerative diseases. *Apoptosis* **29**, 3–21. https://doi.org/10.1007/s10495-023-01902-9 (2024).
28. Chattopadhyay, S., Hazra, R., Mallick, A., Gayen, S. & Roy, S. A review on comprehending immunotherapeutic approaches inducing ferroptosis: managing tumour immunity. *Immunology.* **172**, 547–565. https://doi.org/10.1111/imm.13789 (2024).
29. Wang, M. et al. Long noncoding RNA LINC00336 inhibits ferroptosis in lung cancer by functioning as a competing endogenous RNA. *Cell. Death Differ.* **26**, 2329–2343. https://doi.org/10.1038/s41418-019-0304-y (2019).
30. Xiao, P. et al. Edaravone dexborneol protects against cerebral ischemia/reperfusion-induced blood-brain barrier damage by inhibiting ferroptosis via activation of nrf-2/HO-1/GPX4 signaling. *Free Radic. Biol. Med.* **217**, 116–125. https://doi.org/10.1016/j.freeradbiomed.2024.03.019 (2024).
31. Liu, W. et al. Edaravone ameliorates cerebral ischemia-reperfusion injury by downregulating ferroptosis via the Nrf2/FPN pathway in rats. *Biol. Pharm. Bull.* **45**, 1269–1275. https://doi.org/10.1248/bpb.b22-00186 (2022).
32. Dang, R. et al. Edaravone ameliorates depressive and anxiety-like behaviors via Sirt1/Nrf2/HO-1/Gpx4 pathway. *J. Neuroinflamm.* **19**, 41. https://doi.org/10.1186/s12974-022-02400-6 (2022).
33. Flood, D. & Taylor, C. T. Targeting HIF-1 to treat AML. *Nat. Cancer.* **5**, 821–822. https://doi.org/10.1038/s43018-024-00779-0 (2024).
34. Mitroshina, E. V. & Vedunova, M. V. The role of oxygen homeostasis and the HIF-1 factor in the development of neurodegeneration. *Int. J. Mol. Sci.* **25** https://doi.org/10.3390/ijms25094581 (2024).
35. Wu, Y. et al. Di-(2-ethylhexyl) phthalate exposure leads to ferroptosis via the HIF-1α/HO-1 signaling pathway in mouse testes. *J. Hazard. Mater.* **426**, 127807. https://doi.org/10.1016/j.jhazmat.2021.127807 (2022).
36. Wu, Y. et al. Polystyrenenanoplastics lead to ferroptosis in the lungs. *J. Adv. Res.* **56**, 31–41. https://doi.org/10.1016/j.jare.2023.03.003 (2024).

37. Wu, X. et al. DiDang decoction improves mitochondrial function and lipid metabolism via the HIF-1 signaling pathway to treat atherosclerosis and hyperlipidemia. *J. Ethnopharmacol.* **308**, 116289. https://doi.org/10.1016/j.jep.2023.116289 (2023).
38. Yuan, S. et al. Sorafenib attenuates liver fibrosis by triggering hepatic stellate cell ferroptosis via HIF-1α/SLC7A11 pathway. *Cell. Prolif.* **55**, e13158. https://doi.org/10.1111/cpr.13158 (2022).
39. Cui, Y. et al. ACSL4 exacerbates ischemic stroke by promoting ferroptosis-induced brain injury and neuroinflammation. *Brain Behav. Immun.* **93**, 312–321. https://doi.org/10.1016/j.bbi.2021.01.003 (2021).
40. Citi, S. et al. A short guide to the tight junction. *J. Cell. Sci.* **137** https://doi.org/10.1242/jcs.261776 (2024).
41. Yuan, S. et al. Association of serum occludin levels and perihematomal edema volumes in intracranial hemorrhage patients. *CNS Neurosci. Ther.* **30**, e14450. https://doi.org/10.1111/cns.14450 (2024).
42. Sun, X. et al. Escin avoids hemorrhagic transformation in ischemic stroke by protecting BBB through the AMPK/Cav-1/MMP-9 pathway. *Phytomedicine.* **120**, 155071. https://doi.org/10.1016/j.phymed.2023.155071 (2023).
43. Kollikowski, A. M. et al. MMP-9 release into collateral blood vessels before endovascular thrombectomy to assess the risk of major intracerebral haemorrhages and poor outcome for acute ischaemic stroke: a proof-of-concept study. *EBioMedicine* **103**, 105095. https://doi.org/10.1016/j.ebiom.2024.105095 (2024).
44. Sun, X. et al. Activation of the Epac/Rap1 signaling pathway alleviates blood-brain barrier disruption and brain damage following cerebral ischemia/reperfusion injury. *Int. Immunopharmacol.* **117**, 110014. https://doi.org/10.1016/j.intimp.2023.110014 (2023).
45. Roy-O'Reilly, M. & McCullough, L. D. Sex differences in stroke: the contribution of coagulation. *Exp. Neurol.* **259**, 16–27. https://doi.org/10.1016/j.expneurol.2014.02.011 (2014).
46. MacLellan, C. L., Paquette, R. & Colbourne, F. A critical appraisal of experimental intracerebral hemorrhage research. *J. Cereb. Blood Flow. Metab.* **32**, 612–627. https://doi.org/10.1038/jcbfm.2012.8 (2012).

Author contributions

Conceptualization, J.T.L., and P.Z.; methodology, H.L., X.L. and J.H.W.; investigation, H.L., X.L., M.Z.L., W.X.L., J.H.W., Y.M.H., and H.Q.Y.; writing—original draft preparation, H.L., and X.L.; writing—review and editing, H.L., J.T.L., and P.Z.; supervision, H.L., J.T.L., and P.Z.; funding acquisition, H.L., P.Z., and J.T.L. All authors have read and agreed to the published version of the manuscript.

Funding

This research was funded by Xinxiang Medical University Doctor Support Foundation (XYBSKYZZ201902), Henan Province Foundation for University Key Teacher (2024GGJS088), Natural Science Foundation of Henan Province (242300421199, 235101610002), Henan Key Laboratory of Neurorestoratology (HNSJXF-2021-004), Scientific and Technological Research Project of Henan Provincial Science and Technology Department (212102310835).

Declarations

Competing interests

The authors declare no competing interests.

Additional information

Supplementary Information The online version contains supplementary material available at https://doi.org/10.1038/s41598-025-99187-2.

Correspondence and requests for materials should be addressed to J.L. or P.Z.